

*Supporting Information*

**A-site Non-stoichiometric Defects Engineering  
in  $x\text{Pt-La}_{0.9}\text{Fe}_{0.75}\text{Sn}_{0.25}\text{O}_{3-\delta}$  Hollow Nanofiber  
for High-Performance Formaldehyde Sensor**

Dong Xu<sup>a</sup>, Yumin Zhang<sup>a,\*</sup>, Qin Zhu<sup>b</sup>, ZhenLin Song<sup>a</sup>, Zongming Deng<sup>a</sup>, Baoye Zi<sup>a</sup>,  
Jin Zhang<sup>a</sup>, Jianhong Zhao<sup>a,\*</sup>, Qingju Liu<sup>a,\*</sup>

<sup>a</sup> *Yunnan Key Laboratory for Micro/Nano Materials & Technology, National Center for International Research on Photoelectric and Energy Materials, School of Materials and Energy, Yunnan University, Kunming 650091, P. R. China.*

<sup>b</sup> *Kunming Institute of Physics, Kunming City, Yunnan Province, 650223, P. R. China*

\*Corresponding Author: Yumin Zhang, E-mail: zhangyumin@ynu.edu.cn

Jianhong Zhao, E-mail: aries88323@163.com

Qingju Liu, E-mail: qjliu@ynu.edu.cn.

## S1. Experimental Section

S1.1 Chemicals and Reagents. The reagents required during the experiment included lanthanum nitrate ( $\text{La}(\text{NO}_3)_3 \cdot 6\text{H}_2\text{O}$ ,  $\geq 99.9\%$ ), iron nitrate ( $\text{Fe}(\text{NO}_3)_3 \cdot 9\text{H}_2\text{O}$ ,  $\geq 98.5\%$ ), Tin(IV) chloride pentahydrate ( $\text{SnCl}_4 \cdot 5\text{H}_2\text{O}$ ,  $\geq 99.0\%$ ),  $\text{H}_2\text{PtCl}_6 \cdot 6\text{H}_2\text{O}$  (AR), Polyvinyl pyrrolidone (PVP, average  $M_w \sim 1.3 \times 10^6$ ), ethanol (AR), citric acid ( $\text{C}_6\text{H}_8\text{O}_7 \cdot \text{H}_2\text{O}$ ,  $\geq 99.5\%$ ), N, N-Dimethylformamide (DMF,  $\geq 99.0\%$ ), ethylene glycol ( $(\text{CH}_2\text{OH})_2$ ,  $\geq 99.5\%$ ). All chemicals were purchased from Shanghai Aladdin Chemical Reagent Co., Ltd. The solvent used in the experiment was high-purity deionized water (DI water, 18.25 M $\Omega$  at 25°C).

### S1.2 The synthesis of xPt-LFS hollow nanofiber

All drugs used were of analytical purity (See S1. Experimental Section) and required no further treatment in this work. The xPt-LFS ( $x=0.5\%$ , 1%, 1.5%, 2%) nanofibers were prepared by electrospinning and water bath method. Firstly, 20 mL DMF and 20 mL ethanol were mixed to form solution 1, then 0.17 g  $\text{SnCl}_4 \cdot 5\text{H}_2\text{O}$  and 1.98 g  $\text{La}(\text{NO}_3)_3 \cdot 6\text{H}_2\text{O}$  and 2.02 g  $\text{Fe}(\text{NO}_3)_3 \cdot 6\text{H}_2\text{O}$  were dissolved in solution 1, and stirred at room temperature. After 10 minutes, 2.1 g  $\text{C}_6\text{H}_8\text{O}_7$  was added to solution 1, then placed in the microwave reaction device and kept at 70°C to form solution 2. After 1 h, add 10 ml of solution 2 to the beaker, then add 1g PVP and stir until PVP is completely dissolved to form solution 3. Solution 3 was transferred to the electrospinning machine with a propulsion speed of 0.0005 mm/s under a voltage of 16 KV. The obtained nanofibers film was dried in air at 60°C for 1 h, then crystallized by step-up temperature. The furnace was ramped up in air at 3°C/min to 200°C for 30 min and then ramped up at 5°C/min to 800°C for 2 h to obtain LFS hollow nanofibers.

The crystallized nanofibers were put into ethylene glycol solutions containing different concentrations (0, 0.5%, 1%, 1.5%, 2%) of  $\text{Pt}^{4+}$ , kept at 40°C for 10 min, and then dried at 300°C for 1 h. The samples with different Pt ratios were noted as LFS, 0.5%Pt-LFS, 1%Pt-LFS, 1.5%Pt-LFS, 2%Pt-LFS, and the detailed process is depicted in Fig. S1.

### S1.3 Sensing measurements

Specific quality of xPt-LFS powder and printing oil (Wuhan, Huachuanguike Co., Ltd.) were mixed in a mortar in the ratio of 1:1.5, applied to the substrate by screen printing and then moved to a 300°C muffle furnace to remove the printing oil. The gas-sensitive substrates were mounted in a four-channel gas-sensitive tester (Wuhan, Huachuanguike Co., Ltd.) and kept at 300°C for 24 h to stabilize the resistance curve. Finally, the performance of the gas-sensitive material can be evaluated. The time to recover the resistance of the gas sensor to 90% of the original value is defined as the recovery time; the response value  $S$  is defined as the ratio of the resistance of the sensing electrode in the formaldehyde ( $R_g$ ) to the resistance in air ( $R_a$ ),  $S=R_g/R_a$ . After encapsulating the sensing material with excellent performance into a device and then plugging the pins into the socket of the integrated circuit module, a sensor is made with the input and output functions of the sensor. The input signal comes from a large amount of data generated by the redox reaction between formaldehyde and sensitive material. The calculation of the Microprogrammed Control Unit (MCU) on the circuit board determines the response value, response-recovery time, and other data. It then outputs directly to the desktop software through the interface, as shown in Fig. S1.

The formaldehyde vapor used in the experiments was derived from chemically analytically pure formaldehyde solution (AR, 37%-40%), which contained 10%-13% methanol solution. In order to exclude the influence of methanol gas on the results, we set up a gas selectivity experiment. The formaldehyde vapor was obtained by injecting the formaldehyde solution into an evaporation plate on the test platform through a microinjector, and the formaldehyde vapor was completely dry. All experiments were conducted in dry air (0% RH) except for the experiment testing the effect of relative humidity (RH) on the sensing electrodes. RH% was detected by a commercial humidity sensor placed in a test chamber, and humid air was injected directly into the chamber via an air humidifier and measured when the resistance and humidity had stabilized.

### S1.4 Characterization

The structure of the xPt-LFS was characterized by an X-ray diffraction instrument

(XRD, D/max-2300, Cu K $\alpha$ ,  $\lambda=0.15416$  nm, 5 kV), and the scanning angle was 10°-80°. The samples' surface morphology and lattice analysis were carried out by field emission scanning electron microscopy (SEM, Nova nanoSEM 450) and high-resolution electron transmission electron microscopy (HRTEM, JEM-2100, 200kV). The elemental mapping spectrum was collected through energy dispersive X-ray spectroscopy (EDS) installed on SEM and TEM. The chemical bond state and element content in the sample were calculated by X-ray photoelectron spectroscopy (XPS, Thermo Fisher Science, Al K $\alpha$ , 1486.6 eV). The unpaired electrons in the sample were recorded by Electron Paramagnetic Resonance spectroscopy (EPR, Buker E500, 9.85GHz). The samples' specific surface area and pore size distribution were statically analyzed by N<sub>2</sub> adsorption and desorption analyzer (BET, Beishide Instrument Technology (Beijing) Co. Ltd, 3H-2000PS2). The Fourier transform infrared spectroscopy (FTIR, FTS-40) identified the functional groups of the samples. The thermal stability of the samples during constant temperature heating was evaluated by thermal gravimetric analyzer (TG, MELER/1200H).

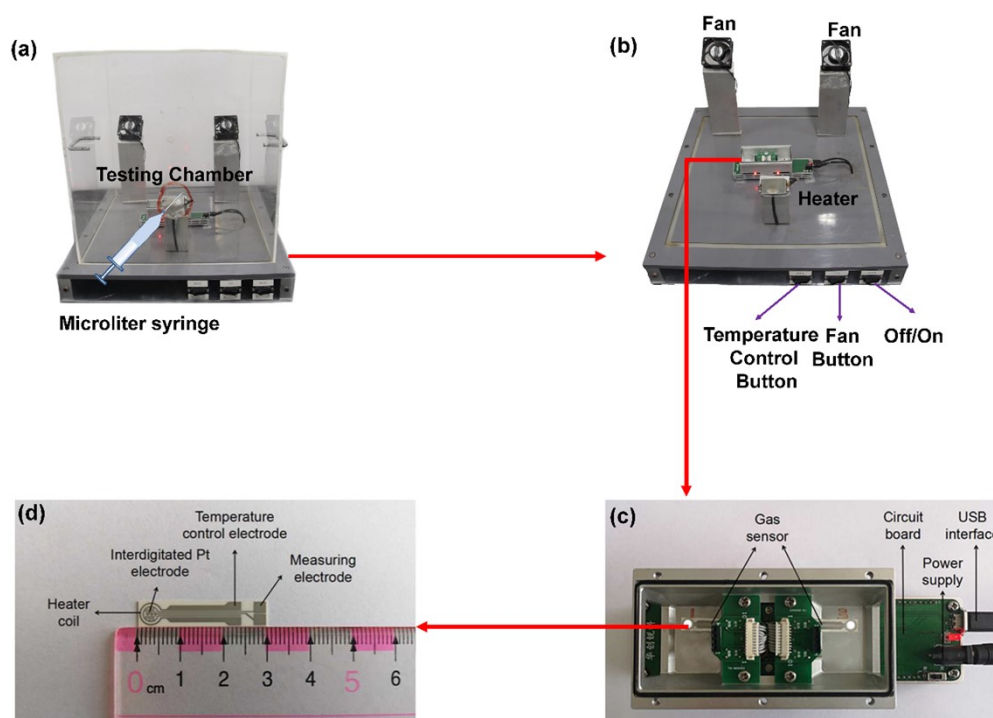


**Fig. S1.** The schematic diagram of gas testing the setup, the gas sensing test (a)

chamber, (b) platform, (c) equipment, (d) substrate.

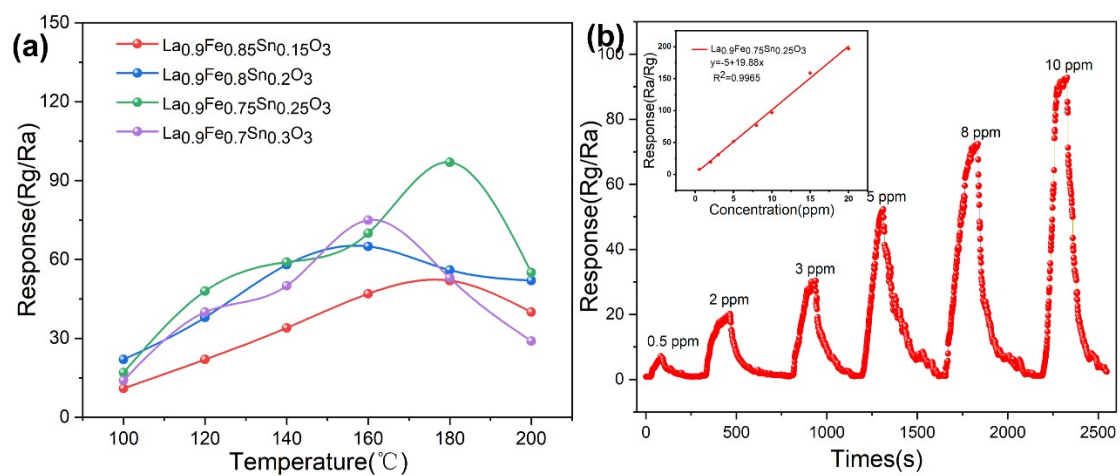


**Fig. S2.** (a)Response of  $\text{La}_{0.9}\text{Fe}_{1-x}\text{Sn}_x\text{O}_{3-\delta}$  to 10 ppm formaldehyde at 100°C-200°C. (b)Dynamic response of LFS to 0.5 ppm-10 ppm formaldehyde at 180°C (inset: a linear fit curve of dynamic response values).

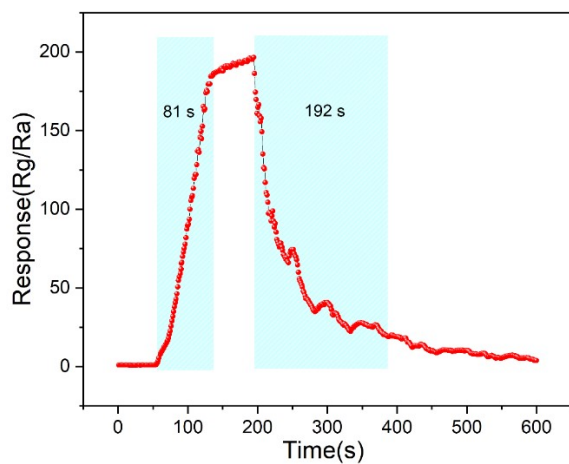


**Fig. S3.** The response-recovery time of LFS to 20 ppm formaldehyde at 180°C.

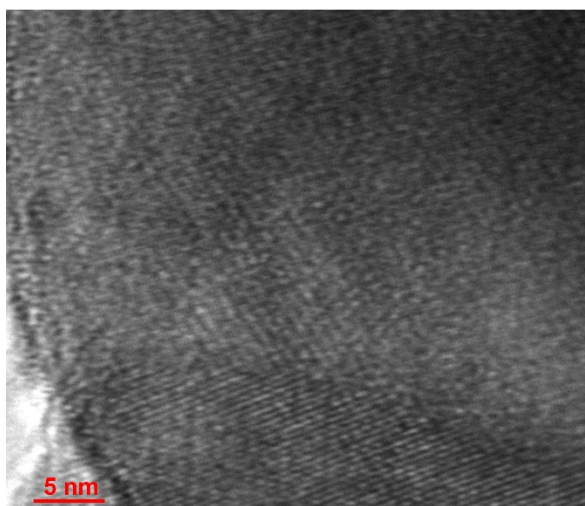


**Fig. S4.** HRTEM image of Pt distribution on LFS nanofiber.

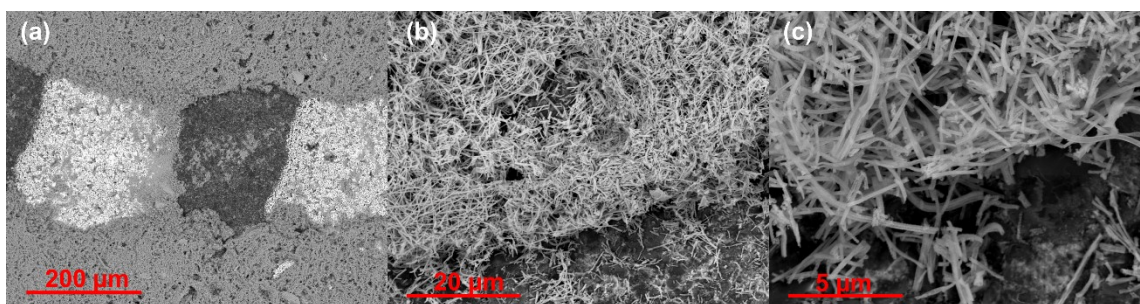


**Fig. S5.** (a-c) A sensitive layer of 1.5%Pt-LFS on a substrate under different magnifications.

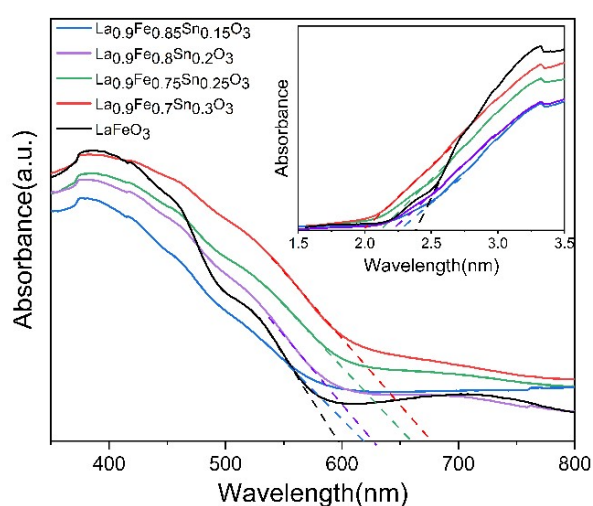


**Fig. S6.** The UV-vis spectrum of  $\text{La}_{0.9}\text{Fe}_x\text{Sn}_{1-x}\text{O}_3$  and the corresponding band width calculated by Kubelka-Munk method.

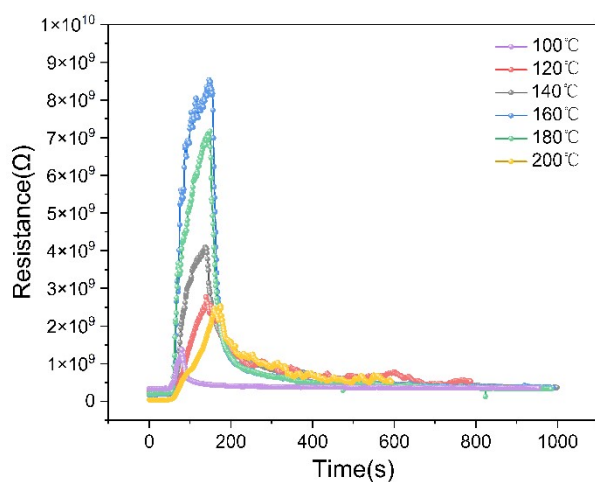


**Fig. S7.** Resistance curve of 1.5%Pt-LFS to 10 ppm formaldehyde at 100°C-180°C.

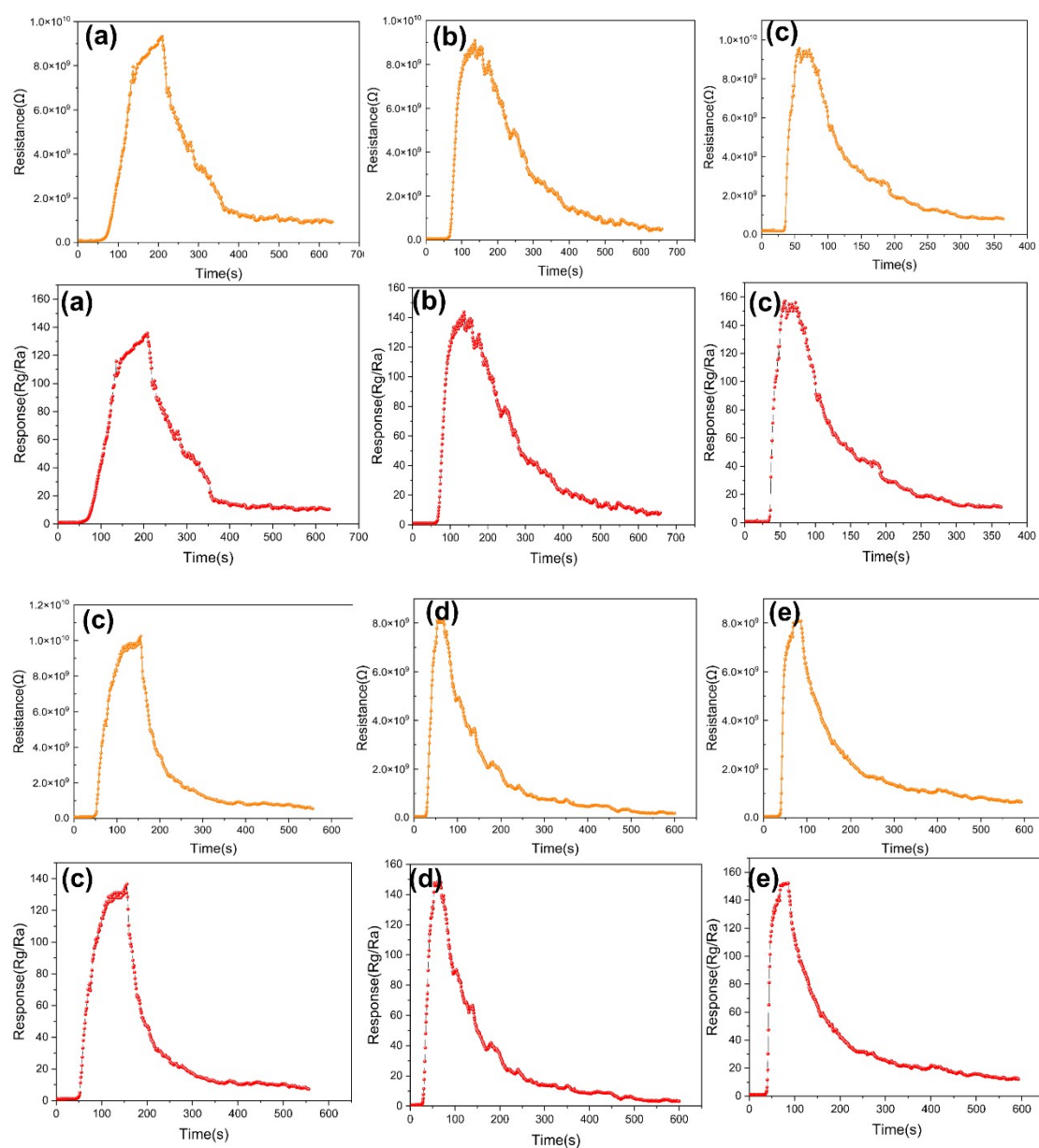


**Fig. S8.** Response value and corresponding response curve of 1.5%Pt-LFS to 10 ppm formaldehyde at an optimum temperature within 26 days.

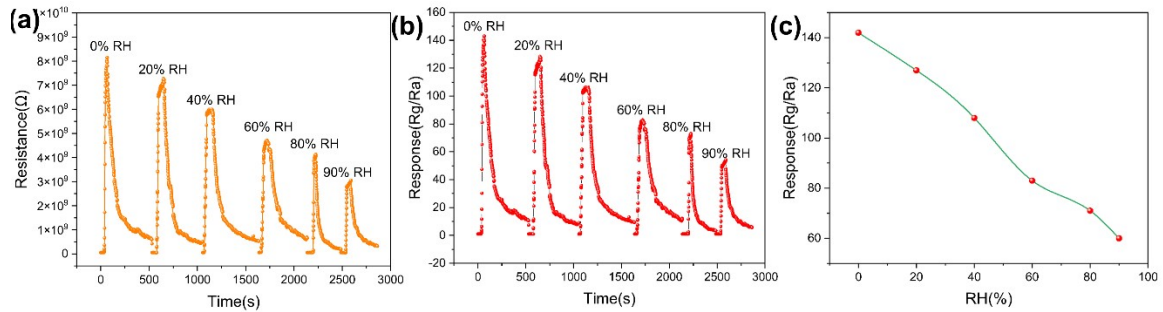


**Fig. S9.** (a) 1.5%Pt-LFS 's resistance change curve to 10 ppm formaldehyde gas under optimal operation and 0-90% RH. (b) Corresponding response-recovery value curves of 1.5%Pt-LFS under 0-90% RH. (c) Curves of changes in 1.5%Pt-LFS response values with increasing RH.



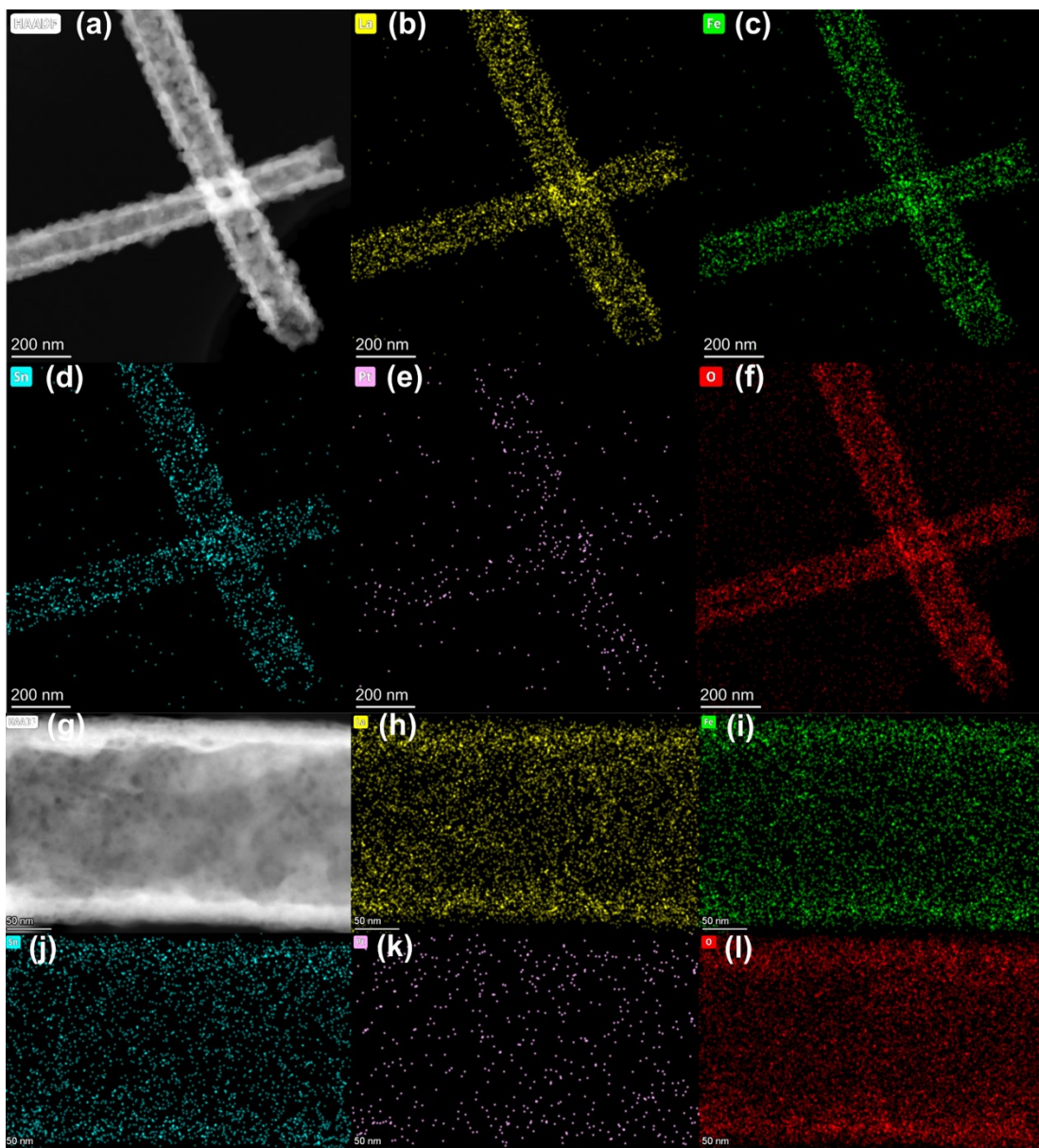


**Fig. S10.** (a, g) STEM-HAADF images and (b-f, h-l) EDS elemental mapping of La, Fe, Sn, O, Pt in 1.5%Pt-LFS.

**Table S1**

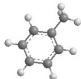
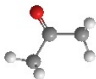




Comparison of formaldehyde sensing performance of various materials reported in recent literature.

Materials	Method	Working temperature (°C)	Formaldehyde (ppm)	Response	Res./Rec. (s)	Ref.

La <sub>x</sub> FeO <sub>3</sub>	Electrospinning technique	180	100	20.4	23/13	1
ZnCo <sub>2</sub> O <sub>4</sub>	Sonication	225	1	7.3	149/497	2
Pt-SnO <sub>2</sub>	Electrospinning technique	275	5	33.9	>5 min	3
Pt- CuBi <sub>2</sub> O <sub>4</sub>	Hydrothermal method	180	5	8	50/53	4
LaFeO <sub>3</sub>	Hydrothermal method	125	50	116	42/55	5
C-LaFeO <sub>3</sub>	Sol-gel method	125	50	74.3	100/20	6
Ag-LaFeO <sub>3</sub>	Electrospinning technique	230	5	4.8	2/4	7
1.5%Pt-LFS	Electrospinning technique	160	20	305	63/151	This work

**Table S2**

Dissociation energy for common sensitive gas molecules<sup>8,9</sup>

Gas	Toluene	Acetone	Methanol	Ethanol	Ammonia	Formaldehyde
Structure						
Bond	CH <sub>3</sub> - C <sub>6</sub> H <sub>5</sub>	H- CH <sub>2</sub> CO CH <sub>3</sub>	H-CH <sub>2</sub> OH	HO-C <sub>2</sub> H <sub>5</sub>	H-NH <sub>2</sub>	H-CHO
Bond Dissociation energy (KJ/mol)	399	393	473	401.2	435	364

## References

- 1 L. Zhu, J. A. Wang, J. W. Liu, X. Chen, Z. C. Xu, Q. Y. Ma, Z. Wang, J. D. Liang, S. S. Li and W. Yan, *Appl. Surf. Sci.*, 2022, **590**, 153085.
- 2 H. J. Park, J. Kim, N. J. Choi, H. Song and D. S. Lee, *ACS Appl. Mater. Interfaces*, 2016, **8**, 3233-3240.
- 3 H. Shin, W. G. Jung, D. H. Kim, J. S. Jang, Y. H. Kim, W. T. Koo, J. Bae, C. Park, S. H. Cho, B. J. Kim and I. D. Kim, *ACS Nano*, 2020, **14**, 11394-11405.
- 4 X. Wang, W. J. Liu, C. L. Wang, S. W. Zhang, M. Ding and X. J. Xu, *Sens. Actuators, B*, 2021, **344**, 130190.
- 5 K. Yang, J. Z. Ma, X. K. Qiao, Y. W. Cui, L. C. Jia and H. Q. Wang, *Sens. Actuators, B*, 2020, **313**, 128022.
- 6 Z. Z. Ma, K. Yang, C. L. Xiao and L. C. Jia, *Sens. Actuators, B*, 2021, **347**, 130550.
- 7 W. Wei, S. J. Guo, C. Chen, L. Sun, Y. Chen, W. B. Guo and S. P. Ruan, *J. Alloys Compd.*, 2017, **695**, 1122-1127.
- 8 J. Carper, *Library Journal*, 1999, **124**, 192-+.
- 9 C. L. Zhang, J. Wang, R. J. Hu, Q. Qiao and X. G. Li, *Sens. Actuators, B*, 2016, **222**, 1134-1143.